Sectional Buckling Tests of Built-up Cold-Formed Steel Columns

Mandana Abbasi[1], Kim J. R. Rasmussen[2], Mani Khezri[3], Benjamin W. Schafer[4]

Abstract

The paper presents tests investigating the local and/or distortional (sectional) buckling of built-up cold-formed steel sections subjected to pure compression. The experiments were designed to study the influence of key parameters, including buckling mode, cross-section geometry and fasteners spacing, on the ultimate sectional capacity of built-up columns. Three singly- or doubly-symmetric built-up sections were tested, comprising two distinct component lipped channel sections; one buckling predominantly in the distortional mode and one buckling predominantly in the local mode. The component sections were connected using self-drilling screws at three different spacings. Material properties, geometric imperfections and residual stresses of the specimens were measured prior to testing. A total of 36 specimens with a length of 1 m were tested under concentric compression between fixed ends. The specimens failed in either distortional or interactive local-distortional buckling modes. Compared to the sum of the capacities of the component sections, the ultimate capacities of the built-up columns failing predominantly in the distortional buckling mode increased significantly with the reduction of screw spacing, whereas the increase was minor for specimens that failed in the interactive local-distortional buckling mode. The ultimate strengths of the specimens are predicted using the current Direct Strength Method, which indicates either conservative or overly unconservative predictions depending on the level of composite action considered in the elastic buckling analysis.

1. Introduction

Cold-formed steel (CFS) sections are extensively used in the low-rise construction industry. CFS applications include roof and wall systems, low-rise residential housing, sheds and industrial portal frames. Built-up cold-formed steel sections offer enormous potential in advancing current and future building practices by extending their applicability range to mid-rise construction. The presence of discrete fasteners influences the member behaviour and might trigger the occurrence of secondary modes. Therefore, a detailed investigation of the buckling behaviour of built-up sections is essential for the safe design and application of this new generation of cold-formed steel sections in low- to mid-rise construction.

---

[1] Research Assistant, The University of Sydney, <mandana.abbasi@sydney.edu.au>
[2] Professor, The University of Sydney, <kim.rasmussen@sydney.edu.au>
[3] Lecturer, The University of Sydney, <mani.khezri@sydney.edu.au>
[4] Professor, Johns Hopkins University, <schafer@jhu.edu>

The early studies on the behaviour of built-up CFS members appear to date back to 1974, when buckling and post-buckling capacities of box and I-columns made of two channels were investigated experimentally (Dewolf 1974). The double-channel CFS beam was analysed by Ghersi et al. (Ghersi 1994) to determine the buckling modes and ultimate behaviour of such beams. Stone and LaBoube (2005) tested the behaviour of an I-section under pin-end conditions and assessed the strength prediction based on the modified slenderness approach in AISI S100 (AISI Standard 2016), which was shown to be conservative. An experimental investigation on screw-connected sigma sections under compression was later carried out by Young and Chen (2008), pointing out the detrimental effect of shear flexibility at the fastener. A series of tests were performed (Reyes 2011) on built-up box sections with fixed and pinned end supports. The results showed that the effect of end boundary conditions on the ultimate loads was insignificant, and the AISI modified slenderness approach could still be used conservatively to design this type of built-up section.

Georgieva et al. performed tests on the behaviour of more complex built-up cross-sections made from two identical lipped Z-sections (Georgieva 2012a) and combinations of three or four Z, C and sigma sections (Georgieva 2012b). The test strengths were affected by slip at fastener points and were shown to be bounded by the design strengths obtained assuming full and no composite action. The effects of various fastener layouts on the capacity of built-up box sections failing in the interactive local-global buckling mode were investigated by Li et al. (2014). The results showed a significant impact of fastener spacing and layout on the failure load. Later, Fratamico et al. (2016) studied the effect of screw spacing on the sectional buckling behaviour of back-to-back channel sections. The test results suggested that increasing the number of equidistant fasteners placed longitudinally did not substantially improve the ultimate capacity of built-up I-sections. However, a compatible web buckling was observed for columns with screw spacing less than $L/4$. A series of compression tests were performed on various screw-connected built-up cross-sections (Craveiro 2016), including back-to-back (I), box (R) and two side-by-side connected box sections (2R), under fixed and pinned end support conditions. The ultimate capacity of the complex built-up 2R-section failing in combined local-global buckling was reported 9.4 and 5.6 times the capacity of its component lipped C-section for pinned- and fixed-ended columns, respectively; values which without partial composite action would have been approximately 4. However, in a subsequent series of stub column tests (Liao 2017) to study the sectional buckling of similar built-up configurations but without the influence of global buckling, the ultimate capacity of the 2R-section was found to be less than or equal to double the capacity of a box section.

The global buckling behaviour of a T-section column composed of three C-sections was investigated by Liu and Zhou (2017), and the results of the strength prediction using (AISI Standard 2016) were found conservative. Subsequently, Lu et al. (2017) studied the buckling behaviour of I-sections with interactive failures, especially local-distortional (LD) and local-distortional-global (LDG) buckling modes. A substantial reduction in the ultimate capacity of built-up I-sections was reported due to the interactive failures. Fratamico et al. (2018a; 2018b) investigated the composite action in screw-connected back-to-back, sheathed and unsheathed channel sections. The results showed that flexural buckling capacity was considerably affected by column end rigidities and the composite action developed through the web screws. Later, Zhang and Young (2018) studied the buckling behaviour of built-up box sections connected with closely-spaced screws, where the governing failure buckling mode was either local or local-flexural.

In recent studies on the buckling of built-up CFS box sections (Roy 2019; Nie 2020a; Nie 2020b; Vy 2021a; Vy 2021b; Zhou 2021) with various lengths and end supports, the impact of fastener spacing on the ultimate capacity was found to be insignificant. In addition, a comprehensive experimental program was carried out to study this impact in more complex built-up sections composed of four component sections (Meza 2020b; Meza 2020a). The maximum increase of the strength of short built-up columns compared to that of a component section was 11%, and the effect of fastener spacing, greater than the local buckle half-wavelength of the section, on the capacity of built-up sections was reported as negligible in general. Phan et al. (2021) studied the local-global buckling behaviour of built-up CFS columns with multiple component sections. It was found that the presence of end fastener groups (EFGs) or more screw rows along the column length does not enhance the ultimate capacity of the columns considerably, and their effect is a function of the end support conditions (Rasmussen 2020). Lastly, the flexural buckling behaviour of two complex closed cross-sections comprising three (Sang 2022) and four (Yang 2022) lipped channel sections were investigated. A noticeable strength enhancement was observed with the reduction of screw spacing.

In summary, previous work on built-up CFS has mainly concerned columns failing by global or local-global interactive buckling and built-up sections comprised of two component sections. It was shown that the local buckling capacity is not meaningfully affected by the presence of fasteners, the influence of fasteners on the global buckling capacity is highly dependent on the end support conditions, and the influence of fasteners on the distortional buckling capacity is potentially significantly enhanced. Therefore, this study aims to provide compression test data for the distortional buckling of built-up CFS sections and its interaction with local buckling in complex built-up sections, mostly comprising more than two component sections. The test results are then used to examine the applicability of the Direct Strength Method (DSM) to the sectional buckling of built-up sections.

2. Experimental Programme
This section covers the details of the tests performed on the sectional buckling of built-up CFS columns. The experimental study was designed to elaborate on the influence of key parameters such as buckling mode, built-up cross-section geometry and fastener spacing.

2.1 Design of test specimens
The main focus of this study is on the sectional buckling of built-up CFS columns; therefore, the individual lipped channel sections were designed to fail through local or distortional buckling modes. A series of elastic buckling analyses were performed using the finite strip method to investigate the effect of cross-section dimensions on the prevalent sectional buckling mode. The parametric study included 162 sections with $E = 210$ GPa and nominal web heights (h) of 100, 150 and 200 mm, lip lengths (b_l) of 10, 15 and 20 mm, nominal thicknesses (t) of 1.2, 1.5 and 1.9 mm and flange widths (b_f) specified with respect to web depths with b_f/h varying from 0.25 to 2. The cross-section was discretised, utilising eight strips in the web and flanges and four strips per lip. The results obtained from the finite strip analyses for $t = 1.5$ mm are presented in Fig. 1; however, additional results for other thicknesses can be found in (Abbasi 2022).

According to the graph, the distortional to local critical buckling stress ratio (f_{crd}/f_{crl}) decreases as the section thickness increases or the lip length decreases. The results also suggest that for the

lipped channel sections with $b_f/h > 1$, the ratio of f_{crd}/f_{crl} tends toward a constant value. A section with a nominal web height of 150 mm and a thickness of 1.5 mm was targeted for selecting the test sections. The remaining sectional parameters were chosen as $b_f/h = 0.8$ and $b_l = 10$ mm, which results in $f_{crd}/f_{crl} = 0.65$, i.e. well below 1.0, to ensure a dominant distortional buckling mode, as shown in Fig. 1. This custom-designed section (referred to as C120) was manufactured by brake pressing high-strength G450 structural steel sheets in a specialised fabrication shop.
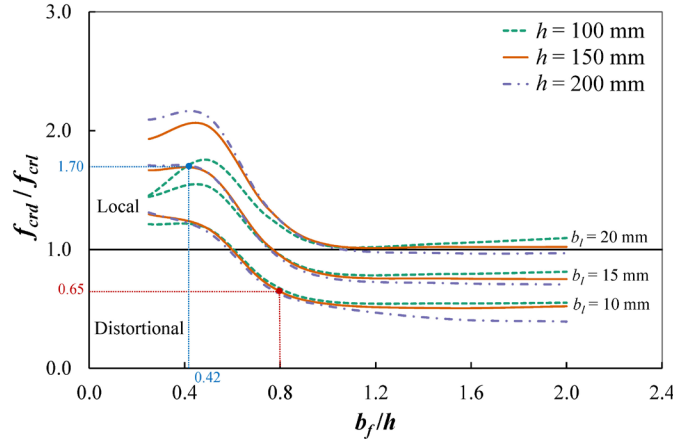

Figure 1: The effect of key sectional parameters on the prevalent sectional buckling mode of lipped channel sections with t = 1.5 mm

The LYSAGHT channel section C15015 (Lysaght 2019) was selected as the next base section for this study, with $b_f/h = 0.42$ and similar nominal height and thickness as the custom-designed sections but a dominant local buckling mode ($f_{crd}/f_{crl} = 1.70$) as depicted in Fig. 1. The LYSAGHT sections (herein referred to as C64) were roll-formed from GALVASPAN steel G450, complying with the Australian standard AS1397-2001 (Australian Standard 2001). The nominal outer dimensions of these two cross-sections are summarised in Fig. 2, in which r_i is the inner radius of the corners. It is noted that the selected sections are identified by their flange width as the main cross-sectional variable.
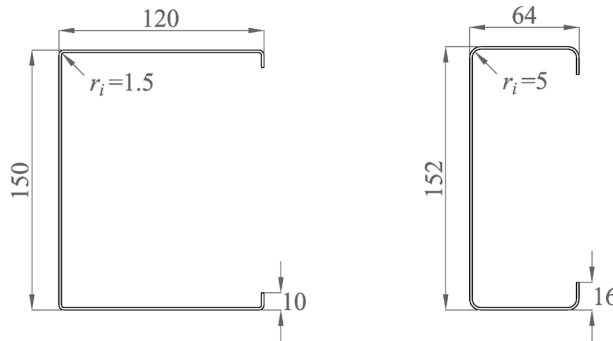

Figure 2: Dimensions of the lipped channel sections designed for testing (in mm)

The nominal length of 1 m was chosen for columns such that one distortional half-wavelength forms along the length of a fixed-ended column. Different singly-symmetric and doubly-symmetric built-up assemblies were then considered comprising two, three and four channel sections (with $h_s = h/6$), as demonstrated in Fig. 3a. The configuration of fasteners along the member

4

length is also schematically drawn in Fig. 3b, where the first row of fasteners was positioned nominally at 50 mm from each end in all configurations.
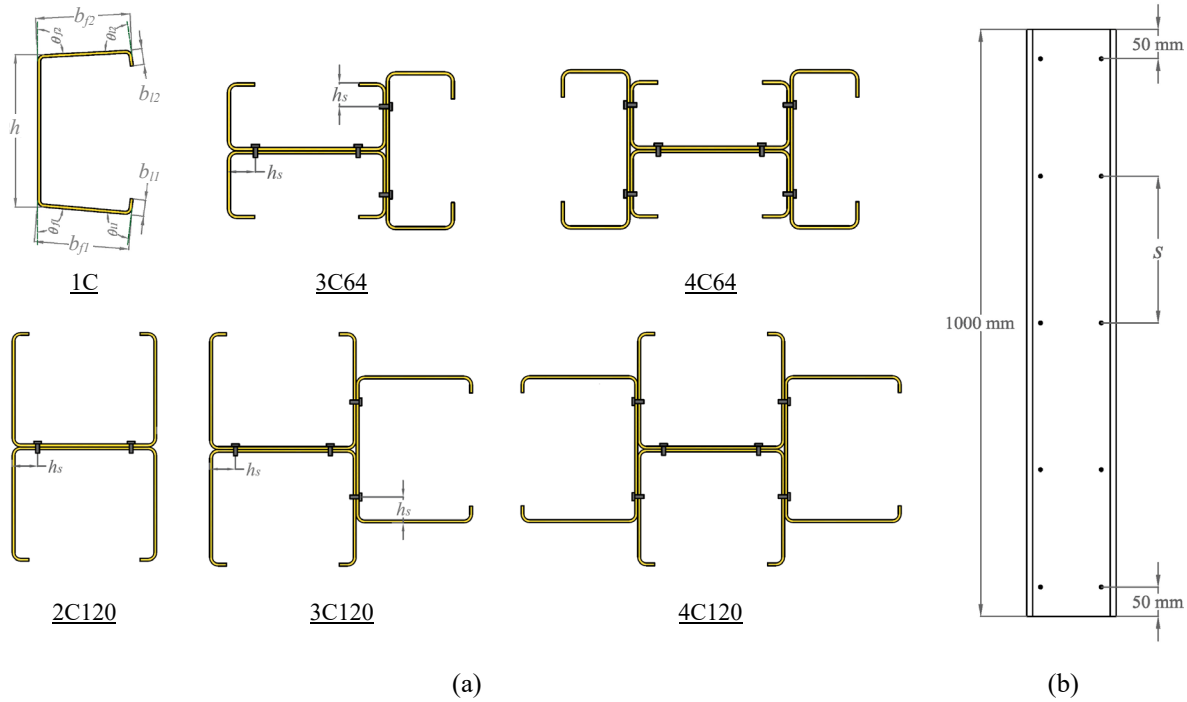

Figure 3: Configuration of built-up test specimens: (a) considered section assemblies, (b) longitudinal fastener arrangement

Through a series of parametric studies using the Compound Strip Method (Abbasi 2018), which the details can be found in (Abbasi 2022), three different spacings were considered in the tests, i.e. $s = 100$, 300 and 900 mm. The variation was considered to study the effect of fastener spacing on the enhancement of the elastic buckling load and the subsequent increase in the ultimate strength capacity of the compression members, especially in distortional buckling mode. In addition, the possibility of secondary local modes with short half-wavelength triggered by discrete fasteners can be investigated. It is also noted that for the experimental study, the back-to-back connected assembly was not considered for section C64 with dominant local buckling mode as the effect of different parameters has already been assessed for this configuration in the literature (Fratamico 2016; Lu 2017; Fratamico 2018a).

2.2 Tensile coupon tests
A total of 24 tensile coupon tests were conducted to quantify the material properties at different parts of the test sections. Tensile coupons were extracted from the web (W), flange (F) and corner (C) of two batches of roll-formed C64 sections and the web and corner of the brake-pressed C120 sections, all cut in the longitudinal direction. Three series of tensile coupon tests were completed to determine the material properties of the flat and corner parts of each channel section. The flat coupon dimensions conformed to the Australian Standard AS 1391 (Australian Standard 2007) and had a nominal width of 12.5 mm and a gauge length of 50 mm. The thickness and the width of each coupon were measured at the centre of the reduced section using a digital vernier before

5

testing. The average flat coupon width and base thickness were 12.32 mm and 1.48 mm, respectively.

For the corner specimens, the coupon width is recommended to be less than the inner corner radius (r_i) for determining the properties of the cold-worked material (Australian Standard 2007). However, adhering to this recommendation for the brake-pressed section was impractical due to its small inner corner radius (r_i = 1.5 mm). Hence, the corner coupon specimens were extracted within the outer corner radius for the brake-pressed section (3 mm wide with a gauge length of 12 mm) and the inner corner radius for the roll-formed section (6 mm wide with a gauge length of 24 mm), conforming to the Australian Standard AS 1391 (Australian Standard 2007). The area of corner coupons was measured according to the weight and density method, as stated in AS 1391 (Australian Standard 2007). The average measured value of the corner coupon area was 9.33 mm^2 and 5.39 mm^2 for C64 and C120 series, respectively.

The tensile coupons were tested in an MTS Criterion testing machine with a capacity of 50 kN according to the Australian Standard AS 1391 (Australian Standard 2007). The tests were operated in a displacement control mode, and the applied displacement rate was 0.2 mm/min for the flat coupons, 0.5 mm/min for the corner coupons of Series C64B1 and 0.4 mm/min for the corner coupons of Series C64B2 and C120. The tests were paused for 2 minutes near the 0.2% proof stress, the ultimate strength and at regular intervals to obtain the material properties at the static equilibrium state. Typical stress-strain curves obtained from sample web and corner coupons are presented for comparison in Fig. 4. As can be seen, the curves follow a similar nonlinear pattern and are also quantitatively comparable in terms of displacement ductility and strength capacities. The complete set of stress-strain curves, including the static and dynamic curves, for all tensile coupon tests from flat and corner material, can be found in (Abbasi 2022).
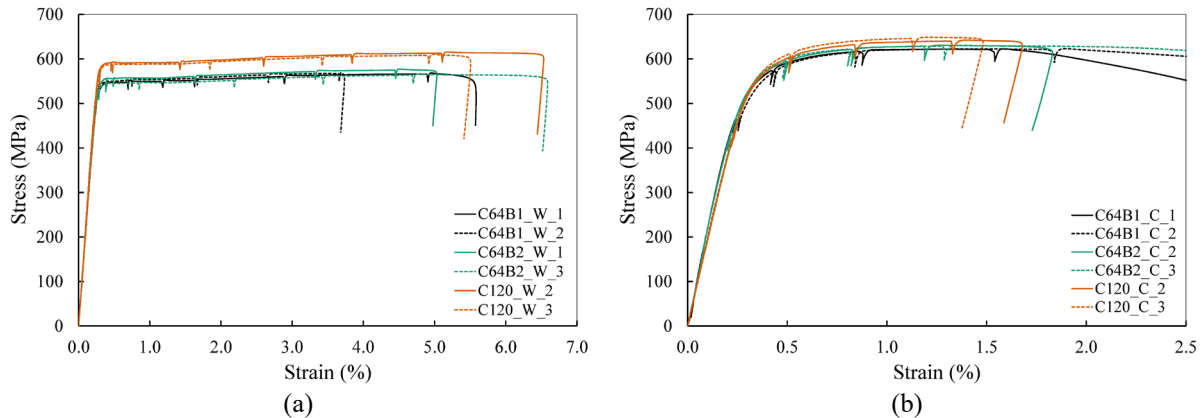

Figure 4: Stress-strain curves of the tested coupons from (a) web and (b) corner

The average values of static material properties of both test series are summarised in Table 1, where E is Young's modulus, $\sigma_{0.01}$ and $\sigma_{0.2}$ are, respectively, the 0.01% and 0.2% proof stresses, and n_{ro} is the strain hardening exponent based on Ramberg-Osgood stress-strain relation (Ramberg 1943). Furthermore, σ_u is the ultimate tensile strength, ε_u is the ultimate strain corresponding to the ultimate stress and ε_t is the total elongation of a gauge length of 50 mm. The results indicate that Series C120, on average, has about 7% and 3% higher 0.2% proof stress ($\sigma_{0.2}$) and ultimate stress (σ_u) capacities than Series C64 for flat and corner parts, respectively.

6

Table 1: Average values of flat and corner material properties

Test series	Location	E (GPa)	$\sigma_{0.01}$ (MPa)	$\sigma_{0.2}$ (MPa)	n_{ro}	σ_u (MPa)	ε_u (%)	ε_t (%)
C120	Flat	216.80	475.6	570.3	16.6	591.4	5.4	10.1
	Corner	191.19	403.6	569.6	8.7	612.1	1.2	3.4
C64	Flat	214.27	461.5	534.4	22.4	552.7	4.7	9.2
	Corner	207.56	398.4	555.1	9.1	596.9	1.5	4.7

Comparing the flat and corner coupon test results shows that the cold-forming process enhances the yield stress and ultimate strength at the corners while decreasing the ductility. It also highlights a more pronounced modification of the average strain hardening exponent from a range of 16.6 to 22.4 for flat parts to a range of 8.7 to 9.1 for the corner coupons, which implies a more rounded stress-strain curve (see Fig. 4).

2.3 Preparation of test specimens
In preparation of the built-up specimens, the individual sections were first cut to length, aligned to the centre of their webs and connected using POWERS #10 hex head self-drilling screws, complying with AS 3566.1 (Australian Standard 2002). The test specimens were then labelled to indicate the primary experimental parameters, *i.e.* the member cross-section, flange width of the channel section and fastener spacing. The specimens were first identified by the number of channel sections included in the member cross-section, "C" referring to a channel section, then the nominal flange width of the channel section in millimetres, followed by the fastener spacing for built-up sections and finally, the specimen number within a group of nominally identical specimens. For instance, 3C120-100-1 is the first specimen of a built-up section comprising three channel sections with a nominal flange width of 120 mm and a fastener spacing of 100 mm.

The outer cross-section dimensions were measured at both ends and the middle of all the component sections of the built-up specimens. The nomenclature for the cross-section dimensions of the component lipped channel section is shown in Fig. 3, where h is the web height, b_{f1} and b_{f2} are the widths of the bottom and top flanges, b_{l1} and b_{l2} are the lengths of the bottom and top lips. The average values of the measured cross-sectional dimensions and their standard deviation for each test specimen are presented in Table 2. The measured widths of the web, flanges and lips are very close to the corresponding nominal values for both the brake-pressed (C120) and roll-formed (C64) sections with a low standard deviation.

To achieve a uniform stress distribution over the member cross-section, both ends of the specimens were flattened using a linisher except for the specimens of Series 4C120, which due to size limit, were instead flattened by an electronic milling machine with a flatness tolerance of ±0.025 mm. In addition, a special end plate was designed for each cross-section, which contained two 16 mm thick steel plates connected using four M12 bolts, as shown in Fig. 5a, to guarantee a fixed-ended boundary condition. The bottom plate was intact, while the cross-section of the specimen with a thickness of 15 mm was extracted from the top plate so that the centroid of the section and the plate coincide.

Each specimen was carefully placed at the centre of the end plates, and the major and minor axes of the cross-section were aligned with the centre lines of the plate. A mixture of Patternstone (ultra-hard gypsum) with a compressive strength of 28 MPa at 1 hour (and 70 MPa at 24 hours) was then

poured into the gap between the section and the end plate and was allowed to set for at least 30 minutes or until it was completely hardened (see Fig. 5b). The specimen was flipped afterwards, and the same procedure was conducted for the other end. Using this type of end plate also facilitates uniform compression loading and prevents localised damage to the section edges at the ends (Yap 2011).

Table 2: Measured cross-sectional dimensions and geometric imperfections of test specimens

| Specimen	Cross-sectional Dimensions					Geometric Imperfections			
	h (mm)	b_{f1} (mm)	b_{f2} (mm)	b_{l1} (mm)	b_{l2} (mm)	Global d_x (mm)	Global d_y (mm)	Distortional (d_f/t)	Local (d_w/t)
2C120-900-1	148.91	120.77	120.69	9.69	9.55	-0.026	0.004	0.366	0.055
2C120-900-2	148.46	120.72	120.76	9.79	10.06	0.034	-0.015	0.396	0.111
2C120-300-1	148.18	120.70	120.84	9.71	9.94	0.031	0.023	0.568	0.077
2C120-300-2	148.20	120.75	120.67	9.71	9.60	0.012	0.062	0.387	0.071
2C120-150-1	148.28	120.61	120.49	9.29	9.94	0.036	0.042	0.492	0.110
2C120-150-2	148.15	120.62	120.54	9.88	9.31	-0.039	0.002	0.327	0.109
2C120-100-1	148.31	120.67	120.62	9.90	9.18	0.010	-0.075	0.245	0.112
2C120-100-2	148.41	120.55	120.51	9.46	9.53	-0.005	0.025	0.480	0.047
3C120-900-1	148.20	120.46	120.45	9.91	9.56	-0.238	0.034	0.155	0.070
3C120-900-2	148.19	120.73	120.58	9.40	9.85	-0.234	-0.017	0.338	0.110
3C120-300-1	148.48	120.72	120.60	9.67	9.48	-0.536	-0.052	0.509	0.193
3C120-300-2	147.88	120.68	120.69	9.65	9.74	-0.180	0.040	0.189	0.063
3C120-100-1	148.67	120.67	120.67	9.58	9.90	-0.163	0.010	0.454	0.118
3C120-100-2	147.80	120.75	120.66	9.75	9.72	-0.105	0.082	0.200	0.111
4C120-900-1	147.69	120.48	120.45	9.93	9.68	0.023	-0.006	0.431	0.181
4C120-900-2	147.51	120.52	120.45	9.85	9.91	-0.019	0.005	0.562	0.102
4C120-300-1	147.15	120.93	120.80	9.75	9.72	-0.007	-0.102	0.505	0.077
4C120-300-2	147.80	120.55	120.50	9.83	9.68	-0.012	-0.038	0.221	0.258
4C120-100-1	147.78	120.55	120.69	9.82	9.55	0.047	-0.037	0.672	0.123
4C120-100-2	147.19	120.80	120.66	9.83	10.00	0.061	0.028	0.616	0.241
Average	148.06	120.66	120.62	9.72	9.70	0.091	0.035	0.406	0.117
St. Dev.	0.45	0.12	0.11	0.17	0.23	0.126	0.027	0.146	0.057
3C64-900-1	153.98	64.54	64.68	15.92	15.87	0.336	-0.104	0.239	0.226
3C64-900-2	154.25	64.52	64.69	16.03	16.38	0.059	0.051	0.213	0.165
3C64-300-1	154.20	64.67	64.75	15.96	15.67	0.100	0.196	0.674	0.279
3C64-300-2	154.01	64.89	64.67	15.79	15.83	0.149	0.072	0.265	0.261
3C64-100-1	153.42	64.01	63.77	15.94	15.72	0.072	0.058	0.322	0.115
3C64-100-2	153.31	63.80	63.99	15.94	15.62	0.154	0.098	0.306	0.194
4C64-900-1	154.11	64.63	64.76	16.01	15.66	0.103	0.039	0.146	0.195
4C64-900-2	154.02	64.62	64.57	15.76	15.93	-0.099	0.024	0.171	0.075
4C64-300-1	154.11	64.54	64.67	15.62	16.00	-0.026	0.076	0.159	0.077
4C64-300-2	154.10	64.69	64.75	15.87	15.86	-0.074	0.107	0.193	0.172
4C64-100-1	154.05	64.68	64.80	15.76	15.54	-0.080	0.028	0.248	0.116
4C64-100-2	153.66	64.53	64.63	16.03	15.60	0.046	-0.049	0.129	0.092
Average	153.94	64.51	64.56	15.89	15.81	0.108	0.059	0.255	0.164
St. Dev.	0.29	0.29	0.31	0.12	0.22	0.071	0.045	0.139	0.067
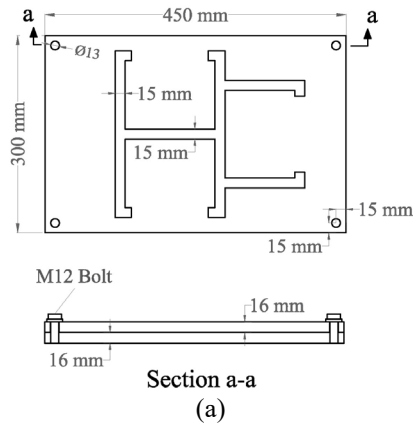
Figure 5: End plate details for a 3C120 built-up specimen: (a) dimensions, (b) actual end support after pouring Patternstone

2.4 Measurement of geometric imperfections

In order to evaluate the shape and magnitude of the imperfections, measurements need to be taken in the transverse and longitudinal directions at discrete points. In this study, laser recording devices were used to measure imperfections. Fig. 6 shows the utilised set-up for measuring the imperfections. The measurement rig consisted of a frame mounted on a trolley and pulled along high-precision guiding bars by a motor. The calibrated laser displacement sensors were connected to the measurement frame using 3 mm steel brackets to measure the absolute distance to the specimen. Since the data sampling rate was 10 Hz, the trolley's speed was set to 10 mm/s, allowing readings every millimetre along the member length. The imperfections were measured at the centre of the web and flanges and 5 mm inwards from the rounded corners and lips. However, because of the impeded access to the web of the built-up sections, the location of the lasers for the top and bottom of the web was adjusted to 30 mm from the centre of the web, which also facilitated investigating the influence of screws on the imperfections.
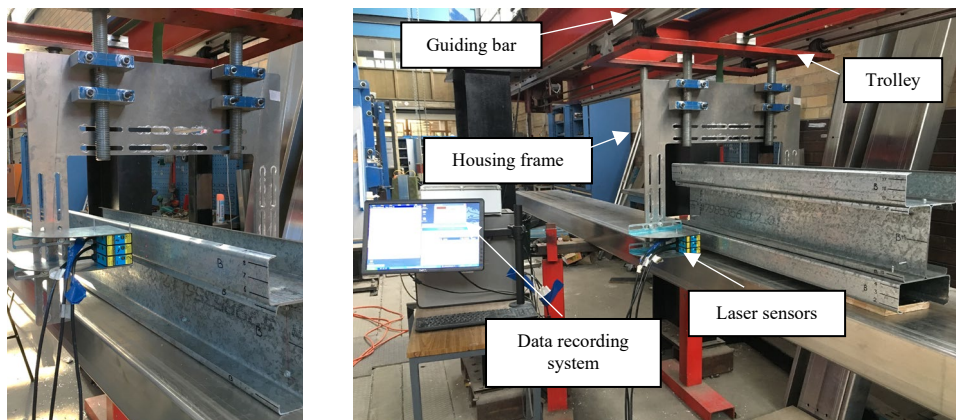

Figure 6: Imperfection measurement rig

Some of the web and flange imperfection readings of specimen 2C120-300-1 are given in Fig. 7 as an indicative example, which desirably shows a negligible noise level from external excitations such as vibrations of the measurement set-up. The locations of fasteners are also indicated in the diagram of web measurements, the effect of which can be observed as a localised disturbance in the overall pattern of imperfections (see Fig. 7a). Note that imperfections were measured on the

9

built-up sections after the installation of fasteners and milling of the ends. The raw data of each line were approximated analytically by sinusoidal Fourier series, partly for convenience in presentation and partly to simplify future use of the measured data. In the Fourier analysis, a total number of 30 sinusoidal terms was retained to eliminate the contribution of high-frequency vibrations while including sufficient terms well beyond the short half-wavelengths associated with local buckling and the minimum fastener spacing in this study (i.e. $s_{min}=L/10$). The approximations of imperfection measurements using finite Fourier series are shown with black lines in Fig. 7, which indicate a good agreement with the measured data. The coefficients of the Fourier approximation of each imperfection reading for all test specimens are listed in (Abbasi 2022).
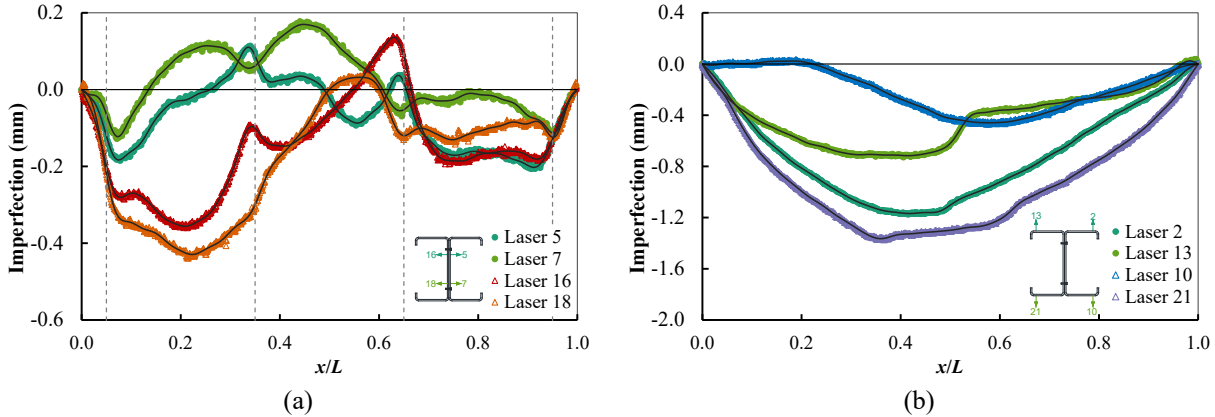

Figure 7: A typical imperfection measurement data with Fourier approximations (black lines): (a) web readings and (b) flange readings

Measured imperfections can be decomposed into the critical eigenmodes of the sections as a common way of incorporating imperfections in numerical modelling (Rasmussen 1988; Schafer 2010; Zeinoddini 2012). In this method, a combination of scaled critical buckling mode shapes of the section is employed to form the imperfection field. For instance, the typical critical buckling mode shapes of a back-to-back I-section are shown in Fig. 8, where d_x and d_y are global imperfections (bow and camber) in x and y directions, and d_w and d_f represent the local and distortional imperfections, respectively. A summary of the representative imperfection parameters obtained from the measured imperfections at the mid-length of each test specimen is listed in Table 2, in which the statistics are based on absolute measured values. Considerable variation in all imperfection parameters was observed, as reflected by a high standard deviation compared to the average values. The global imperfection components about the minor and major axes were fairly small for both test series as the specimens were short and connected back-to-back in built-up assemblies.
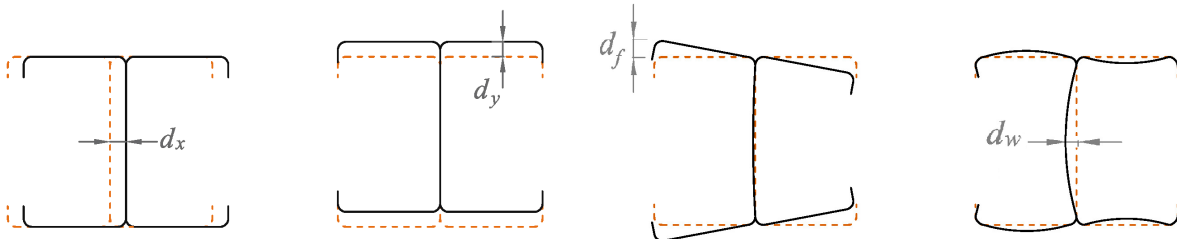

Figure 8: Critical buckling mode shapes of a built-up I-section

10

2.5 Test set-up

All specimens were tested between fixed ends under monotonically increasing concentric compression. The actual test set-up for Series C120 and C64 specimens is shown in Fig. 9a and Fig. 9b, respectively. A 600×300×16 mm steel plate was fixed to the centre of the bottom platen of the testing machine, and the bottom end plate of the specimen was then perfectly aligned with the centre lines of the fixed plate. Once the specimen was set in place, a layer of a thick mixture of Patternstone was poured on top of the end plate at the opposite end (see Fig. 9c), and the loading plate was then moved down gradually to squeeze out the Patternstone layer around the loading plate to provide a uniform compression loading during testing. The Patternstone was allowed to harden fully before applying load.

Linear Variable Displacement Transducers (LVDTs) were mounted on each specimen in the middle of the web and at the junctions of the flanges and lips (with 10 mm clearance from the edge) at two different locations along the member length to monitor local and distortional deformations. The arrangements of transducers around each cross-section and along the member length are presented in Fig. 9a-b. The longitudinal locations were at the mid-height of the specimens, and the distance d_t down from the mid-height. This distance (d_t) was chosen as 100 mm for the specimens of Series C64 such that it was less than the local buckling half-wavelength of the section and provided adequate room for installation. For the specimens of Series C120, this distance was 250 mm, which corresponded to the half-wavelength of the second distortional mode to capture the out-of-plane behaviour of the section in the longitudinal direction. In addition, four transducers were installed on the end plates according to Fig. 9c-d, i.e. two on the bottom end plate and two on the top end plate, close to the centroid of the cross-section, to measure the actual axial shortening of the specimens. Once the transducers had been mounted, displacement-controlled loading was applied to all specimens using a DARTEC testing machine with a 2000 kN capacity with a loading rate of 0.2 mm/min.
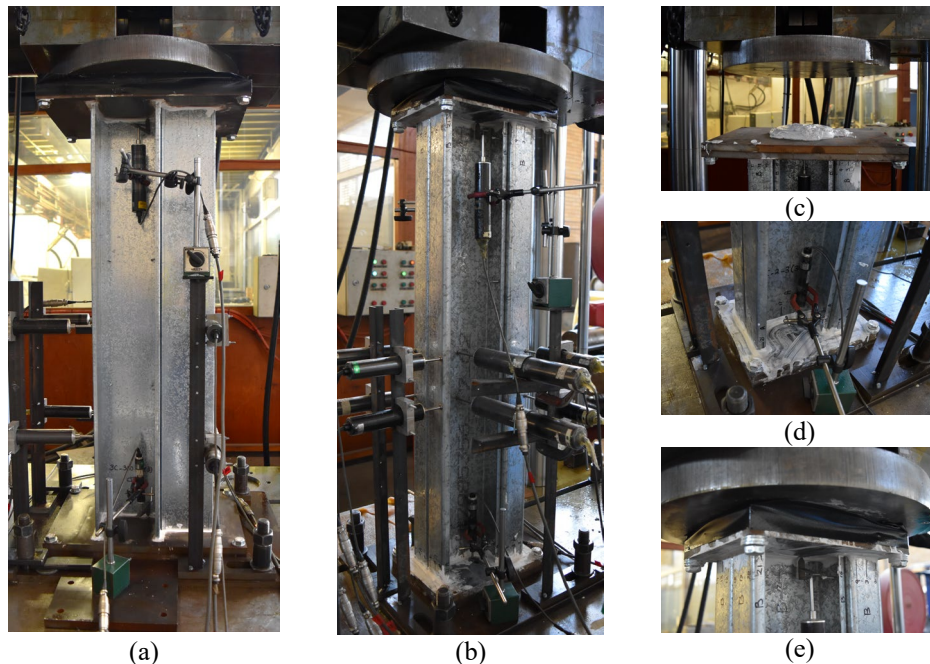

Figure 9: Details of the test set-up: (a) Series C120, (b) Series C64, (c) Patternstone layer between the loading plate and the top end plate, and mounted transducers on the (d) bottom end plate and (e) top end plate

11

3. Results and Discussion

3.1 General test observations

As observed from the tests, all the specimens of Series C120 underwent distortional buckling before reaching the peak load, while local-distortional interactive buckling was prevalent for the Series C64 specimens. As representative examples, Fig. 10 show the transducer measurements at the mid-height of specimens, denoted by 'M', and at the distance of d_t below the mid-height, denoted by 'D', for one of the specimens of 4C configuration from each test series. The sign convention for displacements and the arrangement of transducers around each cross-section are included in the figures. The complete load vs. transducer displacement graphs are presented in (Abbasi 2022).

According to the graphs in Fig. 10a, significant distortional buckling occurred during the testing of C120 specimens with a typical maximum displacement of 25 mm. Following the onset of distortional buckling, large deformations developed in the flanges at the D-location. These large distortional deformations provoked a reversal in the direction of flange movement at the M-location for built-up sections. This result also highlights the change of distortional buckling shape from a single half-wave curve in a channel section, corresponding to the first mode, to an antisymmetric double half-wave curve in built-up sections, corresponding to the second distortional buckling mode. The post-peak buckling deformation of specimen 4C120-300-1 is shown in Fig. 11a.
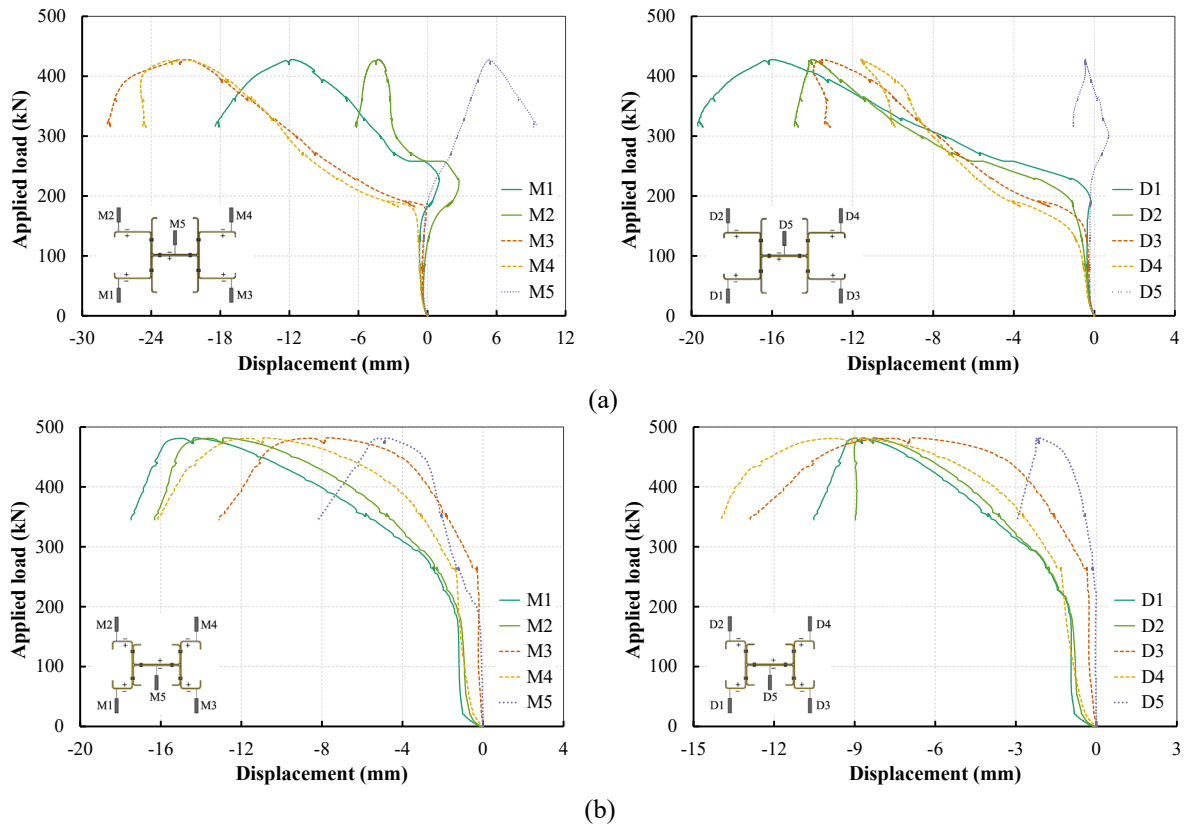

(a)

(b)

Figure 10: Transducers data at mid-height (M) and d_t down from the mid-height (D) for specimen (a) 4C120-300-1 and (b) 4C64-300-1
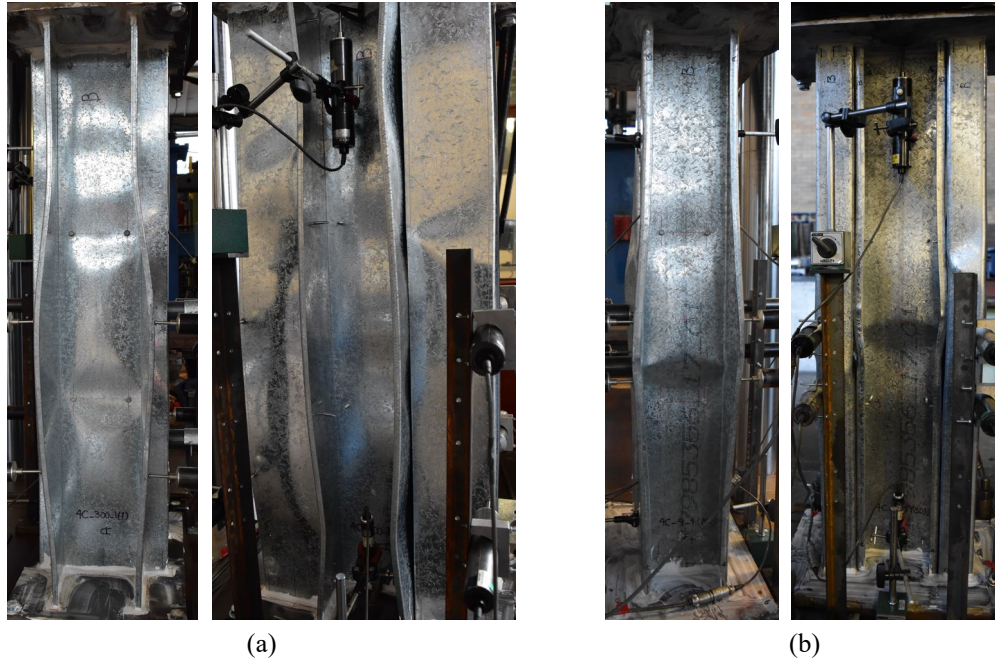
12

Figure 11: Post-peak buckling deformations (front and side views) of the specimen (a) 4C120-300-1 and (b) 4C64-300-1

Fig. 10b shows the occurrence of local buckling in the elastic region of a C64 specimen, recognised by a sharp change in the slope of the load-displacement curves of transducers M5 and D5 mounted on the web at a load of about 190 kN. At this stage, the deformations developed in the flanges of all cross-sections were negligible. However, as the axial load increased, a change occurred in the slope of the load-displacement curves of the transducers mounted on the flanges, which signalled the onset of distortional buckling in the section. Following that, noticeable distortional deformations developed in the flanges before reaching the peak load, indicating the occurrence of failure through the interaction of local and distortional buckling modes. Eventually, the deformations localised somewhere along the length of the column in the post-peak regime, and a flip-disc plastic mechanism formed in the specimens without causing damage to the screws, as shown in Fig. 11b. Similar behaviour was observed for all C64 specimens.

3.2 Ultimate load capacity
The measured data of the four transducers mounted on the top and bottom end plates are utilised to obtain the axial shortening of the specimen along the centroidal line. The load versus axial shortening curves for the 4C specimens are presented in Fig. 12. The recorded load of the single channel sections is multiplied by the number of channel sections included in the section assembly (n=4) and included in the figures for comparison with the results of built-up sections. A summary of test results is also provided in Table 3 for each test specimen, which lists the ultimate static capacity of the section (P_u) and the capacity enhancements relative to the capacity of the single section (P_{u1}) and built-up section with only end fasteners ($P_u|_{s=0.9L}$). According to the results, the ultimate load capacity of the built-up sections increases as the screw spacing decreases. The total capacity enhancement compared to the corresponding component section capacity, i.e. ($\Delta P_u = P_u - nP_{u1})/nP_{u1}$, is more considerable for test specimens of Series C120, which failed in distortional buckling, with a maximum enhancement of 36.5%.
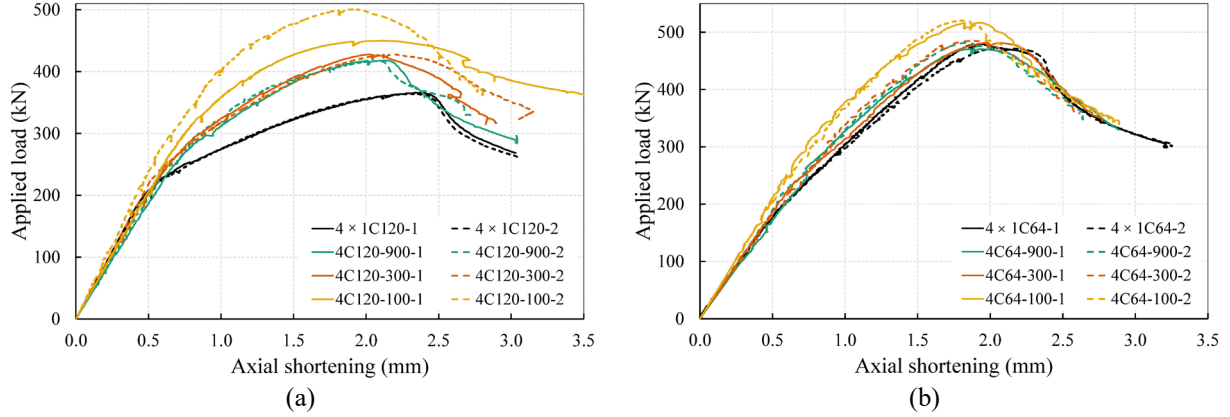
13

Figure 12: Load vs. Axial shortening curves of test specimens (a) 4C120 and (b) 4C64

This total increase in the ultimate capacity includes the effect of end connectivity, intermediate fasteners and any change of mode shape formed in the built-up sections compared to the component section, which may be decomposed into two components; one due to the end connectivity and one due to the intermediate fasteners. The former can be identified as the enhancement of the ultimate capacity of the built-up section with only end fasteners relative to the multiple single-section capacities without interactions, i.e. $(\Delta P_u|_{s=0.9L}=P_u|_{s=0.9L}-nP_{u1})/nP_{u1}$. This enhancement includes the effect of contact initiated between the constituent plates and a potential shift of the buckling mode towards the higher modes in one or multiple individual cross-sections. The second component of the ultimate capacity enhancement, defined as $(\Delta P_{uf} =P_u-P_u|_{s=0.9L})/P_u|_{s=0.9L}$, results from introducing intermediate fasteners and associated reduction in fastener spacing. It follows from Table 3 that by increasing the number of component sections in the built-up section (2C, 3C, 4C), the contribution of end connectivity to the enhancement of the built-up section capacity ($\Delta P_u|_{s=0.9L}/nP_{u1}$) increases considerably (by 4.8%, 9.5%, 14%) for Series C120, in contrast to a marginal increase (less than 2%) for Series C64. Since all the Series C64 sections mostly deformed in the first local buckling mode shape, it can be inferred that the end connectivity and the resultant contact between the sections did not significantly influence the local buckling capacity. Moreover, the addition of evenly-spaced intermediate screws did not significantly improve the ultimate capacity of built-up sections for both test series, with $\Delta P_{uf}/P_u|_{s=0.9L}$ being less than 10%, excluding specimen 4C120-100-2.

3.3 Comparison with DSM predictions
The Direct Strength Method (DSM) correlates the ultimate capacity of the member with the critical elastic buckling loads of the section, which can be obtained from a rational stability analysis, and the yield stress. It has been successfully incorporated into the Australian Standard AS/NZS4600 (Australian Standard 2018) and North American Specification (AISI Standard 2016) to design cold-formed steel structural members. For the use of DSM in the design of built-up sections, the most challenging task is the determination of critical elastic buckling stresses. Due to the inability of the conventional Finite Strip Method (FSM) to explicitly account for discrete fasteners, researchers have trialled various techniques to obtain the critical loads and associated buckle half-wavelengths of built-up sections. A lower-bound estimate of strength can be obtained by assuming no composite action (NC) between component sections, and the theoretical yet practically unachievable upper bound can be obtained by assuming a fully-composite (FC) state with component sections being fused at abutting surfaces.

14

Table 3: Summary of the test results and its comparison with DSM predictions

Specimen	P_u^{exp} (kN)	$\Delta P_u / nP_{u1}$ (%)	$\Delta P_{uf}/ P_u|_{s=0.9L}$[1] (%)	P_u^{design} (kN)		P_u^{exp}/ P_u^{design}	
				NC	FC	NC	FC
2C120-900-1	188.9	4.8	-	198.0	243.8	0.95	0.77
2C120-900-2	199.6	10.8	-	201.4	248.7	0.99	0.80
2C120-300-1	202.2	12.2	7.0	199.4	246.8	1.01	0.82
2C120-300-2	190.4	5.7	0.8	199.1	244.1	0.96	0.78
2C120-150-1	190.8	5.9	1.0	195.7	241.2	0.98	0.79
2C120-150-2	191.2	6.1	1.2	196.5	242.0	0.97	0.79
2C120-100-1	193.0	7.1	2.2	195.9	240.6	0.98	0.80
2C120-100-2	195.2	8.3	3.3	195.7	240.6	1.00	0.81
3C120-900-1	295.9	9.5	-	297.3	391.4	1.00	0.76
3C120-900-2	303.7	12.4	-	295.1	376.4	1.03	0.81
3C120-300-1	300.7	11.2	1.6	295.9	385.0	1.02	0.78
3C120-300-2	299.6	10.8	1.3	297.2	383.8	1.01	0.78
3C120-100-1	317.2	17.4	7.2	299.0	383.3	1.06	0.83
3C120-100-2	322.8	19.4	9.1	297.1	385.4	1.09	0.84
4C120-900-1	411.2	14.1	-	399.2	549.7	1.03	0.75
4C120-900-2	410.7	14.0	-	402.1	547.1	1.02	0.75
4C120-300-1	420.3	16.6	2.3	394.5	543.6	1.07	0.77
4C120-300-2	422.1	17.1	2.8	398.9	543.8	1.06	0.78
4C120-100-1	442.9	22.9	7.8	393.6	537.1	1.13	0.82
4C120-100-2	492.1	36.5	19.8	402.9	543.1	1.22	0.91
3C64-900-1	352.0	0.2	-	333.9	500.0	1.05	0.70
3C64-900-2	358.5	2.0	-	334.2	502.6	1.07	0.71
3C64-300-1	362.4	3.1	2.9	333.0	497.4	1.09	0.73
3C64-300-2	356.3	1.4	1.2	332.2	497.3	1.07	0.72
3C64-100-1	386.8	10.1	9.8	332.7	498.2	1.16	0.78
3C64-100-2	381.0	8.4	8.2	332.5	499.4	1.15	0.76
4C64-900-1	468.8	0.0	-	443.9	681.7	1.06	0.69
4C64-900-2	474.6	1.3	-	443.4	681.3	1.07	0.70
4C64-300-1	477.9	2.0	2.0	443.6	682.0	1.08	0.70
4C64-300-2	477.5	1.9	1.9	444.1	683.0	1.08	0.70
4C64-100-1	505.6	7.9	7.9	441.6	679.5	1.14	0.74
4C64-100-2	513.1	9.5	9.5	444.0	682.5	1.16	0.75

[1] This capacity enhancement is calculated with respect to the minimum capacity of the two nominally identical specimens with a fastener spacing of 0.9*L*.

As required for direct strength design equations, the critical stresses for the local (f_{crl}) and distortional (f_{crd}) buckling modes are evaluated from the signature curves of the component C64 and C120 single-sections under pinned end conditions using the FSM with one longitudinal term (M=1). In addition, the critical buckling stress of the member (f_{cr}) is estimated from the elastic buckling analyses using the FSM under fixed-end conditions with the inclusion of 30 longitudinal terms. The results of the elastic buckling analyses for test specimens (using the measured cross-sectional dimensions and material properties) with different levels of composite action under pinned and fixed end boundary conditions are reported in (Abbasi 2022). For Series C64 test specimens with prevalent local buckling mode, the critical buckling loads under different boundary

conditions were almost identical. However, for distortional buckling, higher buckling loads are achieved for the fixed-ended columns due to the influence of end conditions.

Finally, the critical buckling load were utilised to calculate the nominal sectional capacity of the test specimens using the direct strength equations. The capacity predictions compared to the test strengths are presented in Table 3. The non-composite (NC) approach provides a conservative estimate, especially for closely spaced fasteners, with an average P_u^{exp}/P_u^{design} ratio of 1.03 and 1.10 for the built-up sections of test series C120 and C64, respectively. The main shortcoming is that the NC approach does not distinguish the slenderness difference between the built-up specimens with various fastener spacings and geometry, as reflected by the critical local buckling stress. On the other hand, the fully composite assumption yields highly unsafe predictions for both test series, with an average P_u^{exp}/P_u^{design} ratio of 0.80 and 0.72 for the built-up sections of test series C120 and C64, respectively. These unconservative predictions are due to the inherent optimism in expecting the achievement of full composite behaviour, which cannot be realised under typical fastener configurations and spacings.

4. Conclusions
In order to investigate the sectional buckling behaviour of cold-formed steel built-up columns, two component lipped channel sections were designed, one brake-pressed (C120) with a prevalent distortional buckling mode and one roll-formed (C64) with a predominant local buckling mode. The testing program comprised three singly- and doubly-symmetric built-up assemblies with three different screw spacings ($s = 100$ mm, 300 mm and 900 mm). The material properties and geometric imperfections were measured along the length of the member at different transverse locations on the web, flanges, and lips of the cross-sections. A total of 36 compression tests under fixed-end boundary conditions were carried out, with 14 transducers monitoring displacements of the web and flanges of the cross-sections.

All the Series C120 specimens buckled and failed by distortional buckling, while local elastic buckling was observed for the Series C64 specimens, followed by an interactive local-distortional buckling mode at the ultimate limit state. The results suggest that the ultimate load capacity of built-up columns increases as the screw spacing decreases. This increase is more significant for the Series C120 specimens, with a maximum enhancement of 36.5% compared to a single-section capacity. The ultimate capacities of the built-up sections were also compared with the capacity of specimens with no intermediate connections ($P_u|_{s=0.9L}$) to investigate the effect of adding evenly spaced intermediate fasteners. The results showed that the enhancement of the ultimate capacity of all built-up sections with different geometry due to intermediate fasteners was of limited significance for both test series, with a general increase of less than 10%. Hence, the main cause of the enhanced capacity was the effect of contact between the constituent plates and a potential shift of the buckling mode towards the higher modes in one or multiple component cross-sections.

The test results were then compared against the predictions by the current DSM design equations based on two different levels of composite action. The strength predictions based on the non-composite approach were conservative, while the fully composite assumption yielded highly unsafe predictions. The results indicate the necessity of employing a more accurate partially-composite buckling analysis that accounts for discrete fasteners in determining critical elastic buckling stresses of built-up members.

Acknowledgments

References

Abbasi, M. (2022), *Sectional Buckling of Built-up Cold-formed Steel Columns*, PhD Thesis, The University of Sydney, Sydney.

Abbasi, M., Khezri, M., Rasmussen, K.J.R. and Schafer, B.W. (2018), "Elastic buckling analysis of cold-formed steel built-up sections with discrete fasteners using the compound strip method", *Thin-Walled Structures*. 124, 58-71.

AISI Standard (2016), *North American Cold-Formed Steel Specification for the Design of Cold-Formed Steel Structural Members*, American Iron and Steel Institute (AISI), Washington, DC.

Australian Standard (2001), *Steel sheet and strip—Hot-dip zinc-coated or aluminium/zinc-coated*, Standards Australia, NSW.

Australian Standard (2002), *Self-drilling screws for the building and construction industries - Part 1: General requirements and mechanical properties*, Standards Australia, NSW.

Australian Standard (2007), *Metallic materials—tensile testing at ambient temperature*, Standards Australia, NSW.

Australian Standard (2018), *Cold-formed steel structures*, Standards Australia, NSW.

Craveiro, H.D., Rodrigues, J.P.C. and Laím, L. (2016), "Buckling resistance of axially loaded cold-formed steel columns", *Thin-Walled Structures*. 106, 358-375.

Dewolf, J.T., Pekoz, T. and Winter, G. (1974), "Local and overall buckling of cold-formed members", *Journal of the Structural Division*. 100(10), 2017-2036.

Fratamico, D.C., Torabian, S., Rasmussen, K.J. and Schafer, B.W. (2016). "Experimental investigation of the effect of screw fastener spacing on the local and distortional buckling behavior of built-up cold-formed steel columns", *International Specialty Conference on Cold-Formed Steel Structures*, Baltimore, Maryland, November 9-10.

Fratamico, D.C., Torabian, S., Zhao, X., Rasmussen, K.J.R. and Schafer, B.W. (2018a), "Experimental study on the composite action in sheathed and bare built-up cold-formed steel columns", *Thin-Walled Structures*. 127, 290-305.

Fratamico, D.C., Torabian, S., Zhao, X., Rasmussen, K.J.R. and Schafer, B.W. (2018b), "Experiments on the global buckling and collapse of built-up cold-formed steel columns", *Journal of Constructional Steel Research*. 144, 65-80.

Georgieva, I., Schueremans, L. and Pyl, L. (2012a), "Composed columns from cold-formed steel Z-profiles: Experiments and code-based predictions of the overall compression capacity", *Engineering Structures*. 37, 125-134.

Georgieva, I., Schueremans, L., Pyl, L. and Vandewalle, L. (2012b), "Experimental investigation of built-up double-Z members in bending and compression", *Thin-Walled Structures*. 53, 48-57.

Ghersi, A., Landolfo, R. and Mazzolani, F.M. (1994), "Buckling modes of double-channel cold-formed beams", *Thin-Walled Structures*. 19(2), 353-366.

Li, Y., Li, Y., Wang, S. and Shen, Z. (2014), "Ultimate load-carrying capacity of cold-formed thin-walled columns with built-up box and I section under axial compression", *Thin-Walled Structures*. 79, 202-217.

Liao, F., Wu, H., Wang, R. and Zhou, T. (2017), "Compression test and analysis of multi-limbs built-up cold-formed steel stub columns", *Journal of Constructional Steel Research*. 128, 405-415.

Liu, X. and Zhou, T. (2017), "Research on axial compression behavior of cold-formed triple-lambs built-up open T-section columns", *Journal of Constructional Steel Research*. 134, 102-113.

Lu, Y., Zhou, T., Li, W. and Wu, H. (2017), "Experimental investigation and a novel direct strength method for cold-formed built-up I-section columns", *Thin-Walled Structures*. 112, 125-139.

Lysaght (2019), *Zeds & Cees User Guide for Design and Installation Professionals*, https://cdn.dcs.lysaght.com/download/lysaght-zeds-cees-purlins-and-girts-user-guide.

Meza, F.J., Becque, J. and Hajirasouliha, I. (2020a), "Experimental study of cold-formed steel built-up columns", *Thin-Walled Structures*. 149, 106291.

Meza, F.J., Becque, J. and Hajirasouliha, I. (2020b), "Experimental study of the cross-sectional capacity of cold-formed steel built-up columns", *Thin-Walled Structures*. 155, 106958.

Nie, S., Zhou, T., Eatherton, M.R., Li, J. and Zhang, Y. (2020a), "Compressive behavior of built-up double-box columns consisting of four cold-formed steel channels", *Engineering Structures*. 222, 111133.

Nie, S.F., Zhou, T.H., Zhang, Y. and Liu, B. (2020b), "Compressive behavior of built-up closed box section columns consisting of two cold-formed steel channels", *Thin-Walled Structures*. 151, 106762.

Phan, D.K., Rasmussen, K.J.R. and Schafer, B.W. (2021), "Tests and design of built-up section columns", *Journal of Constructional Steel Research*. 181, 106619.

Ramberg, W. and Osgood, W.R. (1943), *Description of Stress-Strain Curves by Three Parameters*, National Aeronautics and Space Administration Washington DC.

Rasmussen, K.J.R. and Hancock, G.J. (1988), "Geometric imperfections in plated structures subject to interaction between buckling modes", *Thin-Walled Structures*. 6(6), 433-452.

Rasmussen, K.J.R., Khezri, M., Schafer, B.W. and Zhang, H. (2020), "The mechanics of built-up cold-formed steel members", *Thin-Walled Structures*. 154, 106756.

Reyes, W. and Guzmán, A. (2011), "Evaluation of the slenderness ratio in built-up cold-formed box sections", *Journal of Constructional Steel Research*. 67(6), 929-935.

Roy, K., Ting, T.C.H., Lau, H.H. and Lim, J.B.P. (2019), "Experimental and numerical investigations on the axial capacity of cold-formed steel built-up box sections", *Journal of Constructional Steel Research*. 160, 411-427.

Sang, L., Zhou, T., Zhang, L., Chen, B. and Wang, S. (2022), "Experimental investigation on the axial compression behavior of cold-formed steel triple-limbs built-up columns with half open section", *Thin-Walled Structures*. 172, 108913.

Schafer, B.W., Li, Z. and Moen, C.D. (2010), "Computational modeling of cold-formed steel", *Thin-Walled Structures*. 48(10), 752-762.

Stone, T.A. and LaBoube, R.A. (2005), "Behavior of cold-formed steel built-up I-sections", *Thin-Walled Structures*. 43(12), 1805-1817.

Vy, S.T. and Mahendran, M. (2021a), "Behaviour and design of slender built-up nested cold-formed steel compression members", *Engineering Structures*. 241, 112446.

Vy, S.T., Mahendran, M. and Sivaprakasam, T. (2021b), "Built-up nested cold-formed steel compression members subject to local or distortional buckling", *Journal of Constructional Steel Research*. 182, 106667.

Yang, J., Xu, L., Shi, Y. and Wang, W. (2022), "Experimental and Analytical Study of Flexural Buckling of Cold-Formed Steel Quadruple-Limb Built-Up Box Columns", *Journal of Structural Engineering*. 148(1), 04021228.

Yap, D.C.Y. and Hancock, G.J. (2011), "Experimental Study of High-Strength Cold-Formed Stiffened-Web C-Sections in Compression", *Journal of Structural Engineering*. 137(2), 162-172.

Young, B. and Chen, J. (2008), "Design of Cold-Formed Steel Built-Up Closed Sections with Intermediate Stiffeners", *Journal of Structural Engineering*. 134(5), 727-737.

Zeinoddini, V.M. and Schafer, B.W. (2012), "Simulation of geometric imperfections in cold-formed steel members using spectral representation approach", *Thin-Walled Structures*. 60, 105-117.

Zhang, J.H. and Young, B. (2018), "Experimental investigation of cold-formed steel built-up closed section columns with web stiffeners", *Journal of Constructional Steel Research*. 147, 380-392.

Zhou, X., Xiang, Y., Shi, Y., Xu, L. and Zou, Y. (2021), "Simplified design method of cold-formed steel columns with built-up box sections", *Engineering Structures*. 228, 111532.